Effects of Synchronous Motors Parameters Variations on Efficiency Maps

Amina Bensalah, Habibou Lawali Ali, Abed Al Kader Al Asmar, Yacine Amara, and Georges Barakat

Abstract This contribution presents a study of the effect of synchronous motors losses parameters variations on the machines behaviour. In particular, the effects on efficiency maps are investigated. The goal is to identify parameters sets allowing improving energy efficiency for a given application.

1 Introduction

Energy efficiency is a very significant issue nowadays, thanks to its direct link to pollution and green gazes' emissions reduction. Any system or device should be designed not only according to envelopes requirements but also considering its behaviour along its lifetime [1].

Electrical traction vehicles are a typical application in which energy efficiency is very important. Indeed, up–to-date batteries still suffer from a relatively low energy density [2]. It is then very important to have the most efficient traction system in order to increase the autonomy of such vehicles, and increase their attractiveness.

First, the model used to conduct this study is presented. Parameters variations are then discussed. The way efficiency maps are estimated will be clearly explained, and the parametric studies are conducted. Finally, some conclusions are drawn based on the effects of losses parameters variations on the efficiency maps.

A. Bensalah · H. Lawali Ali · A. A. K. Al Asmar · Y. Amara (✉) · G. Barakat
GREAH Groupe de Recherche en Electrotechnique et Automatique du Havre, EA 3220, Université Le Havre Normandie, Le Havre, France
e-mail: amina.bensalah@g.enp.edu.dz; habibou.lawali-ali@doct.univ-lehavre.fr; abed-al-kader.al-asmar@univ-lehavre.fr; yacine.amara@univ-lehavre.fr; georges.barakat@univ-lehavre.fr

W. Zamboni, G. Petrone (eds.), *ELECTRIMACS 2019*, Lecture Notes in Electrical Engineering 615, https://doi.org/10.1007/978-3-030-37161-6_13

2 Synchronous Motors Model

The conventional first harmonic model defined in the synchronous d–q reference frame, including iron loss [3–5], is used in this study. The magnetic saturation is neglected. Nevertheless, the effect of magnetic saturation could be studied via its impact on machines inductances. Hybrid excitation synchronous machines (HESM) model being the more general synchronous machines model is used as the base of this study. The models of other synchronous machines, PMSM (permanent magnet synchronous machine), electrically excited machines and synchronous reluctance machines, could all be easily derived from the HESM model.

Figure 1a–c show d–q equivalent circuits of the armature windings, and the wound field excitation equivalent circuit, respectively.

More details about this model could be found in [5]. Symbols in Fig. 1 are defined as:

i_d, i_q	d and q components of armature current
I_e	current in excitation windings
$i_{\mathrm{f}d}$, $i_{\mathrm{f}q}$	d and q components of iron loss current
v_d, v_q	d and q components of terminal voltage
V_e	excitation voltage
R_a	armature windings resistance per phase
R_f	iron loss resistance
R_e	excitation winding resistance
Φ_a	permanent magnet flux linkage
Φ_exc	total excitation flux linkage
k_e	mutual inductance between the armature and the excitation windings
L_d, L_q	d and q components of synchronous inductance

2.1 Per-Unit System

The per-unit system defined in [5] is briefly recalled in this section. It allows a better understanding of parameters effect on machines performance. It also constitutes a powerful tool for electric machines classification [6–8]. Base values of EMF, current and mechanical speed Ω_b are chosen as the reference values. More details could be found in Ref. [5]. Per-unit formula for the armature current and the terminal voltage are given by

$$I_n = \frac{\sqrt{i_d^2 + i_q^2}}{I_\mathrm{m}} \tag{1}$$

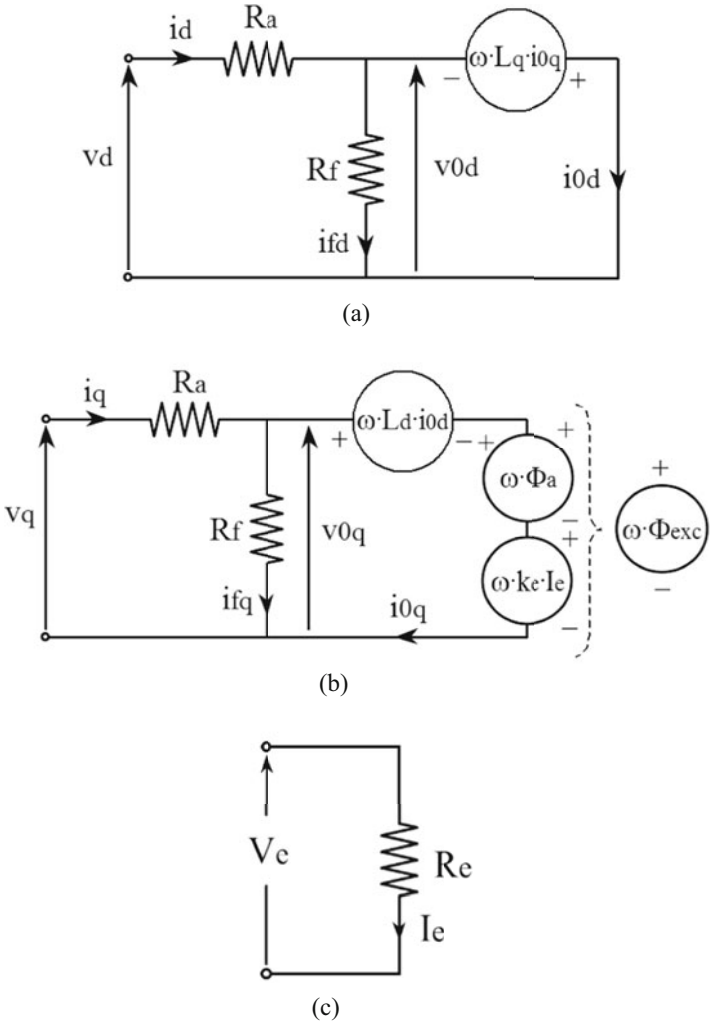

Fig. 1 Synchronous machines equivalent circuits. (**a**) Equivalent circuit in *d* axis. (**b**) Equivalent circuit in *q* axis. (**c**) Equivalent circuit of the wound field excitation

$$V_n = \frac{\sqrt{v_d^2 + v_q^2}}{\Phi_{\mathrm{e\,max}} \cdot p \cdot \Omega_{\mathrm{b}}} \tag{2}$$

where,

I_{m}: armature current maximum value (*d*–*q* referential),
p: number of pole pairs,

Ω_b: base speed (rated speed),
$\Phi_{e\,max}$: total excitation flux maximum value.

Per-unit values are defined using subscript n. Per-unit expressions of some quantities are defined by Eq. (3):

$$\Omega_n = \frac{\Omega}{\Omega_b},\ P_n = \frac{P}{V_m \cdot I_m} \text{ and } T_n = \frac{P_n}{\Omega_n} \tag{3}$$

where V_m is the maximum applied armature voltage (in d–q referential).

Per-unit values of the excitation current and the mutual inductance between the excitation and the armature windings are given by

$$I_{en} = \frac{I_e}{I_{em}} \text{ and } k_{en} = \frac{k_e \cdot I_{em}}{\Phi_{e\,max}} \tag{4}$$

where,

I_{em}: maximum excitation current,

The saliency ratio ρ has also to be defined ($=L_q/L_d$). Furthermore, the excitation coefficient k_f, linking the total excitation flux with the maximum flux linkage, is defined by

$$\Phi_{exc} = \Phi_a + k_e \cdot I_e = k_f \cdot \Phi_{e\,max} \tag{5}$$

The excitation coefficient varies ideally between 0 and 1. However, the thermal constraints, demagnetization limits and/or the magnetic saturation could limit the possibility of cancelling the PM excitation flux ($k_{f\,min} > 0$).

Hybridization ratio α, which is a parameter specific to HESM and which offers an additional degree of freedom, is given by

$$\alpha = \frac{\Phi_a}{\Phi_{e\,max}} \tag{6}$$

Using Eqs. (4), (5) and (6), k_f could be expressed as a function of the normalized excitation current:

$$k_f = \alpha + k_{en} \cdot I_{en} \tag{7}$$

2.2 Parameters variations

Table 1 gives normalized parameters variations intervals. These intervals are bounded by values between which the different parameters could reasonably vary.

Table 1 Normalized parameters variations intervals

Parameter	Variations interval
L_{dn}	[0, 5]
ρ	[0, 5]
R_{an}	[0, 0.5]
R_{fn}	[5, $+\infty$]
R_{en}	1
k_{en}	[0, 1]
β	[5, $+\infty$[

Main parameters of the various types of synchronous motors are given by

$$\begin{cases} \text{Wound field excited motors} & \Rightarrow (\alpha = 0, k_{en} \neq 0) \\ \text{PM excited motors} & \Rightarrow (\alpha = 1, k_{en} = 0) \\ \text{Synchronous reluctance motors} & \Rightarrow (\alpha = 0, k_{en} = 0) \\ \text{Hybrid excited motors} & \Rightarrow (\alpha \neq 0, k_{en} \neq 0) \end{cases} \tag{8}$$

β the power rating ratio of converters connected to both the armature windings and excitation coils, needs to be defined for wound field and hybrid excitation machines. It is given by

$$\beta = \frac{V_{\mathrm{m}} \cdot I_{\mathrm{m}}}{V_{\mathrm{em}} \cdot I_{\mathrm{em}}} \tag{9}$$

where, V_{em} is the maximum excitation coil terminal voltage. More details are provided in [5].

Machines where losses are neglected have $R_{\mathrm{a}} = 0\ \Omega$ and $R_{\mathrm{f}} \rightarrow +\infty\ \Omega$. For PM excited and synchronous reluctance machines $\beta = +\infty$.

3 Efficiency Maps Computation

Efficiency maps represent a practical way to evaluate motor designs [5, 9–12]. Efficiency maps estimation is based on the algorithm shown in Fig. 2. Per-unit value of speed varies between 0 and $\Omega_{n\max} > 1$, and T_n could vary between 0 and 1. The algorithm helps identify (k_{f}, I_n, ψ) combination, which maximizes efficiency for each (Ω_n, T_n) combination. ψ is the phase shifting between the EMF and the armature current. For each operating point, three imbricated loops allow identifying (k_{f}, I_n, ψ) combinations, which meet the (speed, torque) demand and the current and voltage limits. Then, the combination of (k_{f}, I_n, ψ) that maximize the efficiency is selected. For the operating points with unfounded combination of (k_{f}, I_n, ψ) that respect the voltage limit, the efficiency is set to 0. Efficiency maps are obtained by displaying iso-lines of efficiency. It should be highlighted that mechanical losses are neglected.

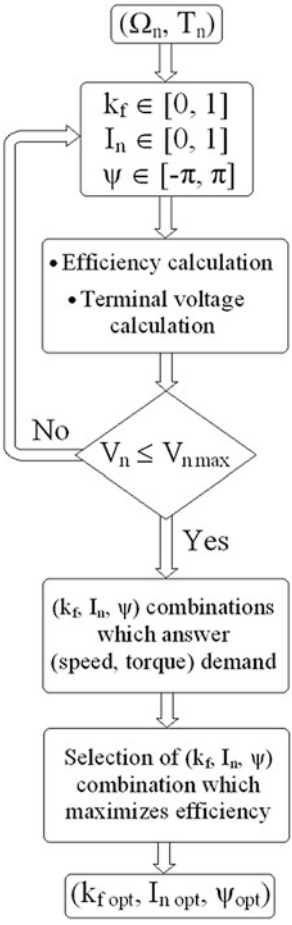

Fig. 2 Efficiency maps computation algorithm

Figure 3 shows efficiency maps for a wound field synchronous motor (Fig. 3a), a PM motor (Fig. 3b) and a hybrid excited motor (Fig. 3c). Only excited synchronous machines are considered because, if well designed, they should have higher efficiencies as compared to non-excited synchronous machines, i.e., synchronous reluctance machines. Efficiency estimation in these figures do not include mechanical and the static converter losses.

The values of the different parameters are given as follows: $L_{dn} = 0.5$; $\rho = 1$; $R_{an} = 0.1$; and $R_{fn} = 20$. For the wound field and the hybrid excited machines, additional parameters are given as follows: $k_{en} = 1$; $R_{en} = 1$; $\beta = 27$, and $\alpha = 1$ for the hybrid excited machine. These parameters are derived from an existing prototype [5, 13].

As could be expected, the PM and hybrid excited motors have higher efficiency as compared to the wound field motor. While the high efficiency zones are located

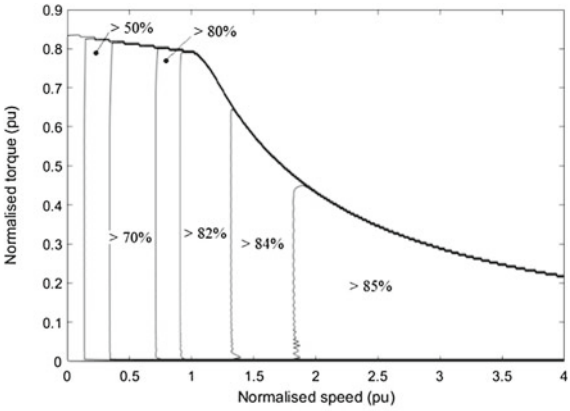

(a)

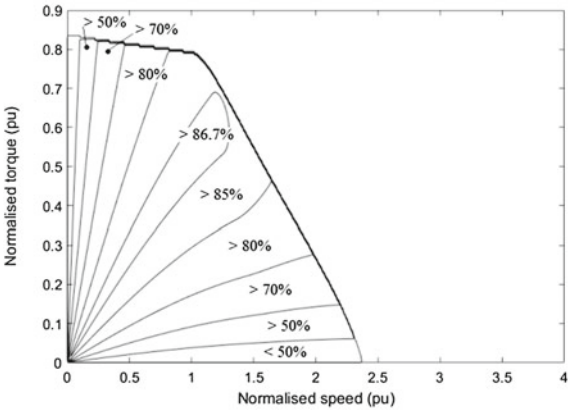

(b)

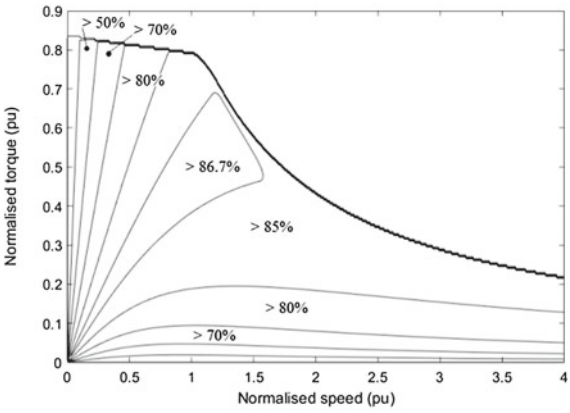

(c)

Fig. 3 Efficiency maps of the different machines. (**a**) Wound field machine. (**b**) PM machine. (**c**) Hybrid excited machine

at high speed for the wound field motor, they are located around the base speed for the PM and the hybrid excited motors.

4 Parametric Study

The parametric study presented in this section is conducted in order to establish the separate effects of each parameter on the efficiency maps. At this stage, only losses parameters are considered, i.e., R_{an} and R_{fn}.

Figure 4 shows the efficiency maps when R_{an} is null, all other parameters are kept equal to previously defined values. As can be seen the efficiency is obviously increasing for same operating conditions as compared to maps shown in Fig. 3. In high-excitation flux requiring regions, the wound field machine has a lower efficiency, as could be expected, since the excitation flux is obtained at the price of excitation joule losses. For the PM machine, the lowest efficiency zones are located in regions where the flux weakening is demanding. The HES machine combines the advantages of both the previous structures. For all machines, the power capability at relatively low speed is increased.

Figure 5 shows efficiency maps when $R_{an} = 0.5$, all other parameters being kept equal to previously defined values. The maximum efficiency is decreasing as expected. It is also the case of the maximum power capability at relatively low speed for all machines. However, it has been observed that the power capability at higher speed has been enlarged for the PM machine [8]. As previously observed, while the high-efficiency zones are located at high speed for the wound field motor, they are located around the base speed for the PM and the hybrid excited motors.

Figure 6 shows efficiency maps when $R_{fn} = 10{,}000$, all other parameters being kept equal to previously defined values ($R_{an} = 0.1$). Having such a high value of R_{fn} means that the iron loss is neglected. It could be observed that if the iron losses are neglected, or insignificant, the torque envelope at low speed is independent of speed. The efficiency is of course higher as compared to maps shown in Fig. 3. The maximum power capability is slightly improved. The reachable speed for the PM machine is not significantly affected.

Figure 7 shows efficiency maps when $R_{fn} = 5$, all other parameters are kept equal to previously defined values ($R_{an} = 0.1$). R_{fn} has a significant effect on the torque envelope slope at low and high speeds. The maximum torque increases at very low speed when R_{fn} decreases. The maximum efficiency zones are shifted to low speed regions. The maximum reachable speed for PM machine decreases as the value of R_{fn} decreases (increasing iron loss). The effect of R_{fn} on this speed seems less important as compared to the effect of R_{an}.

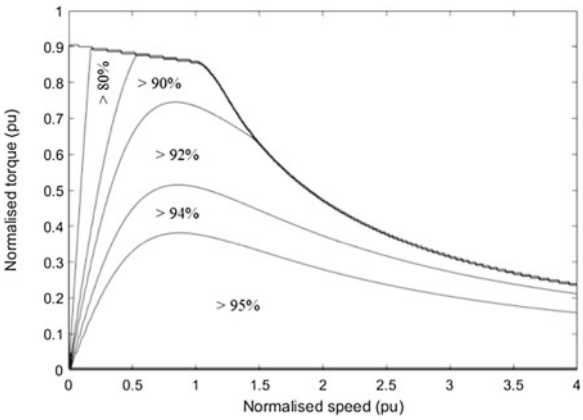

(a)

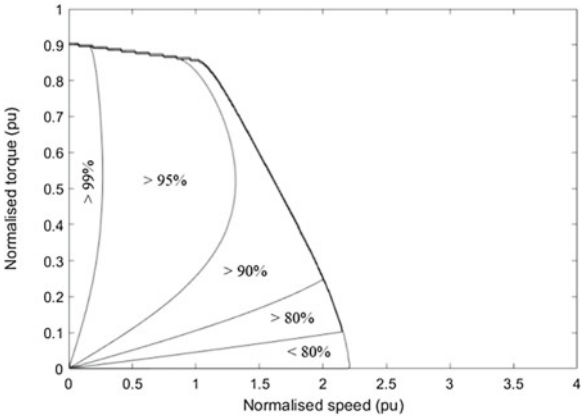

(b)

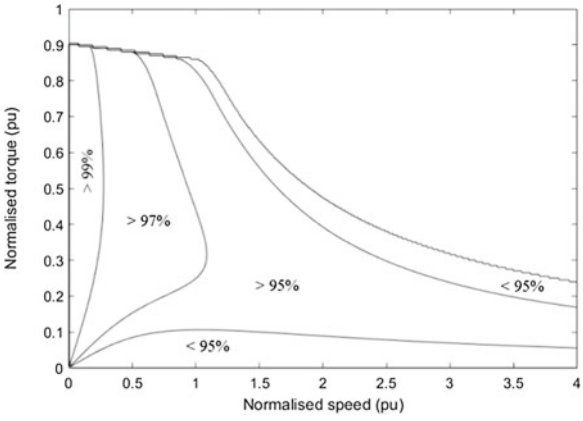

(c)

Fig. 4 Efficiency maps of the different machines when $R_{an} = 0$. (**a**) Wound field machine. (**b**) PM machine. (**c**) Hybrid excited machine

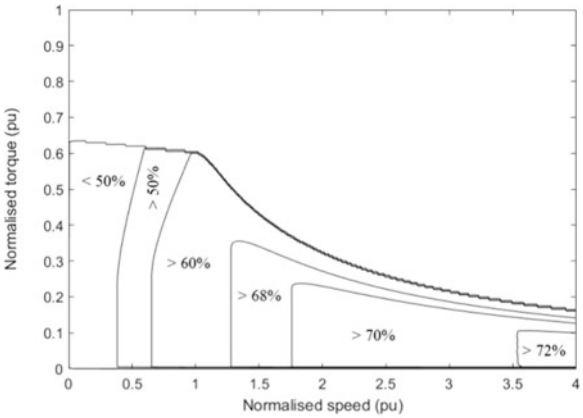

(a)

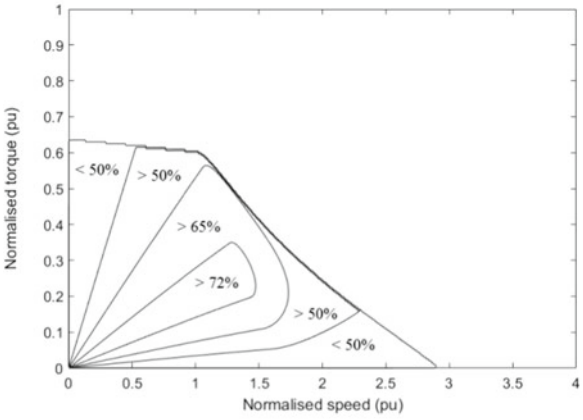

(b)

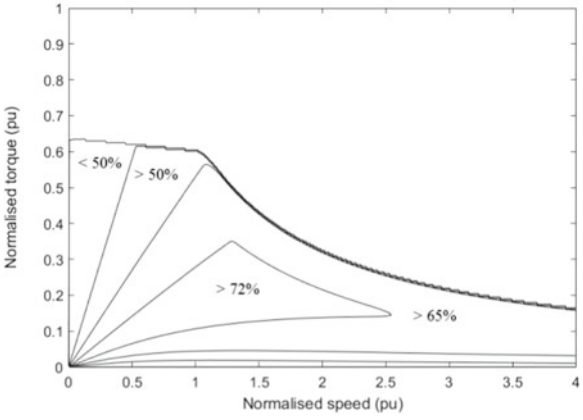

(c)

Fig. 5 Efficiency maps of the different machines when $R_{an} = 0.5$. (**a**) Wound field machine. (**b**) PM machine. (**c**) Hybrid excited machine

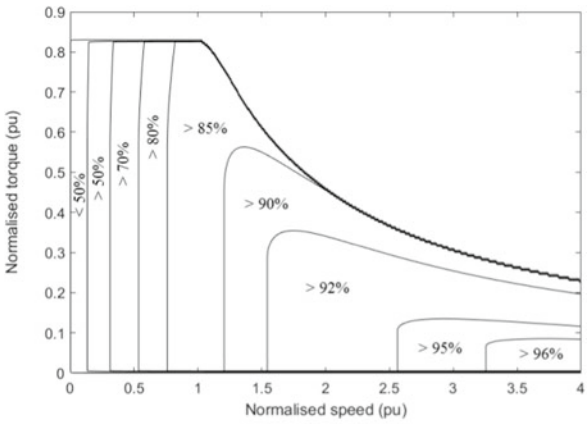

(a)

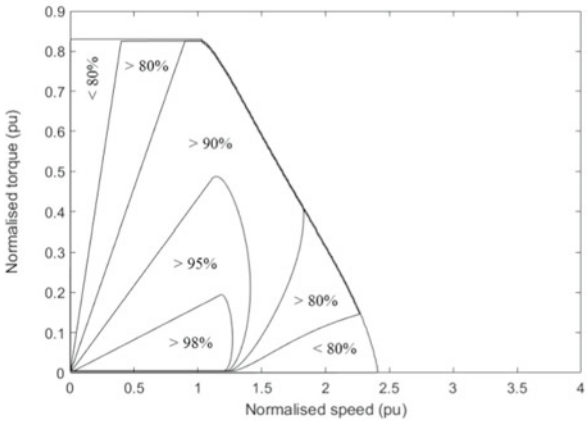

(b)

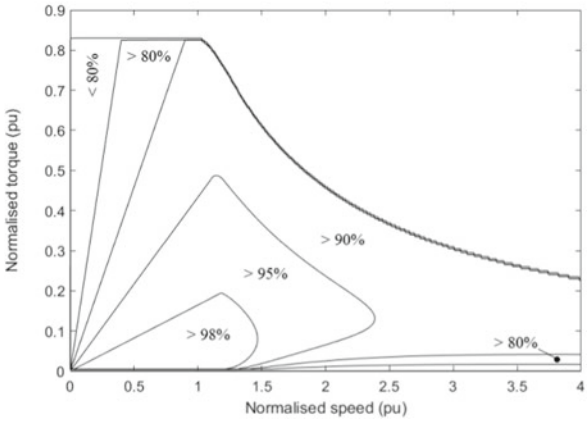

(c)

Fig. 6 Efficiency maps of the different machines when $R_{fn} = 10{,}000$. (**a**) Wound field machine. (**b**) PM machine. (**c**) Hybrid excited machine

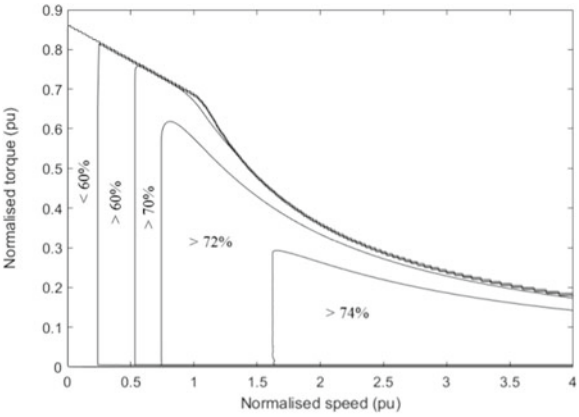

(a)

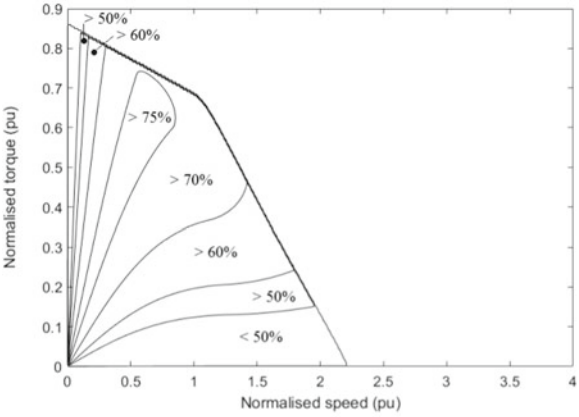

(b)

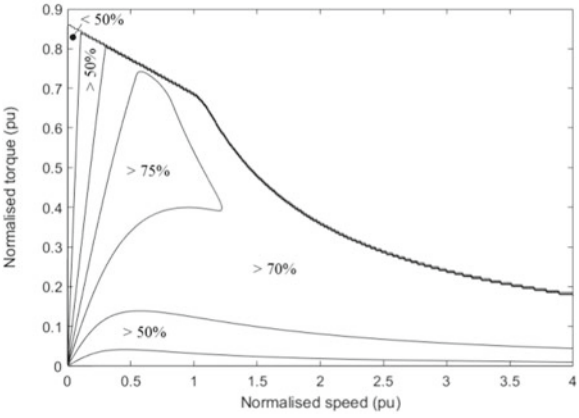

(c)

Fig. 7 Efficiency maps of different machines when $R_{fn} = 5$. (**a**) Wound field machine. (**b**) PM machine. (**c**) Hybrid excited machine

5 Conclusions

A parametric study has been conducted in order to evaluate the effects of losses parameters, i.e., R_{an} and R_{fn}, on the efficiency maps of excited synchronous motors. Interesting features have been identified concerning the behaviour of the PM machine operation at high speeds. It has been observed that the maximum reachable speed increases when the value of R_{an} increases. The maximum power capability is obviously reduced at relatively low speed when R_{an} increases. The maximum reachable speed for the PM machine when the iron loss increases (R_{fn} decreasing) is decreasing. The power capability at low speed is less affected by the variations of R_{fn}, as compared to variations of R_{an}.

All observations show that the established tool is consistent with scientific literature. It constitutes therefore a very interesting tool to explore different characteristics and extend the parametric study.

This study should be regarded as a general theoretical analysis of the effect of synchronous machines parameters on efficiency maps. The use of normalized parameters, and quantities, was aiming at serving this goal. An experimental validation was not pursued, since only tendencies were sought. Nevertheless, the used tool was previously compared to a corresponding experimental study in [5]. In order to link this theoretical study to real design considerations, here are described the effects of some general design considerations on the two considered parameters, i.e., R_{an} and R_{fn}:

1. The reduction of armature resistance could be sought by the use of concentrated tooth windings with reduced end-windings. The use of an adapted cooling can also help keep the windings temperature as low as possible to avoid increasing the windings resistivity.
2. The reduction of iron loss could be achieved by using low iron loss ferromagnetic materials grades. In contrast to joule losses, the temperature increase induces a reduction of iron loss.

References

1. G. Choi, T.M. Jahns, Design of electric machines for electric vehicles based on driving schedules, in *Proceedings of 2013 International Electric Machines & Drives Conference (IEMDC2013)*, Chicago, IL, USA, 12–15 May 2013, pp. 54–61
2. M. Yilmaz, P.T. Krein, Review of battery charger topologies, charging power levels, and infrastructure for plug-in electric and hybrid vehicles. IEEE Trans. Power Electron. **28**(5), 2151–2169 (2013)
3. S. Morimoto, Y. Tong, Y. Takeda, T. Hirasa, Loss minimization control of permanent magnet synchronous motor drives. IEEE Trans. Ind. Electron. **41**(5), 511–517 (1994)
4. F. Fernandez-Bernal, A. Garcia-Cerrada, R. Faure, Determination of parameters in interior permanent-magnet synchronous motors with iron losses without torque measurement. IEEE Trans. Ind. Appl. **37**(5), 1265–1272 (2001)

5. Y. Amara, L. Vido, M. Gabsi, E. Haong, A.H. Ben Ahmed, M. Lécrivain, Hybrid excitation synchronous machines: energy-efficient solution for vehicles propulsion. IEEE Trans. Veh. Technol. **58**(5), 2137–2149 (2009)
6. R.F. Schiferl, T.A. Lipo, Power capability of salient pole permanent magnet synchronous motors in variable speed drive applications. IEEE Trans. Ind. Appl. **26**(1), 115–123 (1990)
7. W.L. Soong, T.J.E. Miller, Field-weakening performance of brushless synchronous AC motor drives. IEE Proc. Electr. Power Appl. **141**(6), 331–340 (1994)
8. J. Soulard, B. Multon, Maximum power limits of small single-phase permanent magnet drives. IEE Proc. Electr. Power Appl. **146**(5), 457–462 (1999)
9. S.S. Williamson, S.M. Lukic, A. Emadi, Comprehensive drive train efficiency analysis of hybrid electric and fuel cell vehicles based on motorcontroller efficiency modeling. IEEE Trans. Power Electron. **21**(3), 730–740 (2006)
10. Y. Sugii, M. Yada, S. Koga, T. Ashikaga, Applicability of various motors to electric vehicles, in *Proc. 13th Int. EVS*, Osaka, Japan, Oct 1996, pp. 757–764
11. A. Fonseca, C. Chillet, E. Atienza, A.-L. Bui-Van, J. Bigeon, New modelling methodology for different PM motors for electric and hybrid vehicles," in *Proc. IEEE Int. Electr. Mach. Drives Conf.*, Cambridge, MA, June 2001, pp. 173–178
12. M. Menne, J. Reinert, R.W. De Doncker, Energy-efficiency evaluation of traction drives for electric vehicles," in *Proc. 15th EVS*, Brussels, Belgium, Oct 1998, 7 pages, CD-ROM
13. Y. Amara, E. Hoang, M. Gabsi, M. Lécrivain, A.H. Ben Ahmed, S. Dérou, Measured performances of a new hybrid excitation synchronous machine. EPE J. **12**(4), 42–50 (2004)